The EMBO Journal Vol.18 No.21 pp.6073–6083, 1999

Identification of RNA-binding surfaces in iron regulatory protein-1

Pierre Kaldy, Eric Menotti, Rémy Moret and Lukas C.Kühn[1]

Swiss Institute for Experimental Cancer Research (ISREC), Genetics Unit, CH-1066 Epalinges, Switzerland

[1]Corresponding author
e-mail: lukas.kuehn@isrec.unil.ch

P.Kaldy and E.Menotti contributed equally to this work

Post-transcriptional regulation of mRNA translation and stability in iron metabolism involves the interaction between the *trans*-acting cytoplasmic iron regulatory proteins (IRP-1 and IRP-2) and *cis*-acting iron-responsive elements (IREs) in mRNA 5′- or 3′-untranslated regions. IRP-1 can adopt two conformations: one with a [4Fe–4S]-cluster, unable to bind IREs, which functions as a cytoplasmic aconitase; one lacking this cluster, which accumulates in iron-deprived cells and binds mRNA firmly. We investigated which surfaces of IRP-1 interact with IREs. Surface areas were predicted on the basis of the crystallized porcine mitochondrial aconitase structure. We selected nine sequences absent or different in mitochondrial and *Escherichia coli* aconitases, both being devoid of RNA-binding properties. Mutations in two regions of domain 4 of IRP-1 lowered the affinity for a wild-type IRE up to 7-fold *in vitro*, whereas the aconitase activity, a control for structural integrity, was not affected. Scatchard plot analysis with mutant IREs indicated that domain 4 is involved in the binding specificity. This conclusion was confirmed with hybrid proteins in which IRP-1 surface loops were grafted into IRP-2. The results indicate that arginines 728 and 732 contact the IRE bulge, whereas region 685–689 is necessary for recognition of the IRE loop.

Keywords: iron regulatory protein/iron-responsive element/mutagenesis/post-transcriptional regulation/RNA–protein interaction

Introduction

The fate of RNA—its processing, transport, localization, translation and degradation—is mostly controlled by the interaction with specific proteins. However, only a very limited number of RNA–protein complexes have been accessible to high-resolution structural studies by co-crystallization or NMR (Nagai, 1996; Uhlenbeck *et al.*, 1997): complexes of certain tRNA/amino acyl-tRNA-synthetases (Biou *et al.*, 1994), U1 snRNA with U1A protein (Oubridge *et al.*, 1994) or MS2 bacteriophage RNA with its coat protein (Valegard *et al.*, 1994). For the iron-responsive element (IRE)–iron regulatory protein (IRP) complex, such approaches have not yet been successful. The prediction of this RNA–protein interaction also remains largely inaccessible, in spite of the recent IRE structure determination by NMR (Laing and Hall, 1996; Addess *et al.*, 1997; Gdaniec *et al.*, 1998) and the knowledge that IRPs belong to the aconitase protein family (see below). The protein contains no known RNA recognition motifs such as those of ribonucleoproteins (Kenan *et al.*, 1991; Burd and Dreyfuss, 1994), the double-stranded RNA-binding domain (Bycroft *et al.*, 1995) or the K homology domain (Siomi *et al.*, 1994; Musco *et al.*, 1996). In this case, the only immediately accessible approach for the determination of RNA-binding sites resides with site-directed mutagenesis.

Iron regulatory protein-1 (IRP-1) is a conditional cytoplasmic mRNA-binding protein, which becomes active under low iron conditions and binds to IRE hairpin loops present in certain mRNA 5′- or 3′-untranslated regions (Casey *et al.*, 1988; Leibold and Munro, 1988; Koeller *et al.*, 1989; Müllner *et al.*, 1989; Hentze and Kühn, 1996). IREs always contain a six-nucleotide loop with the sequence CAGUGN (where N is any nucleotide except G) at the end of a stem of five paired nucleotides. The loop-nucleotides in positions 1 and 5 interact through their base (Henderson *et al.*, 1994; Laing and Hall, 1996; Addess *et al.*, 1997; Gdaniec *et al.*, 1998). Next to the 5′-end of the stem there is invariably an unpaired C, which is part of an asymmetric bulge that is closed by additional paired nucleotides. Binding of IRP-1 to 5′-IREs blocks translation of mRNAs coding for H and L ferritins, mitochondrial aconitase, erythroid 5-aminolevulinate synthase and succinate dehydrogenase subunit b of *Drosophila melanogaster* (Hentze and Kühn, 1996). In contrast, binding to five 3′-IREs in transferrin receptor mRNA correlates with the stabilization of this mRNA (Casey *et al.*, 1988; Müllner *et al.*, 1989), presumably by preventing its cleavage by an endoribonuclease (Müllner and Kühn, 1988; Binder *et al.*, 1994). Under high iron conditions, IRP-1 dissociates from IREs and is converted to a cytoplasmic aconitase through insertion of a [4Fe–4S]-cluster (Haile *et al.*, 1992; Kennedy *et al.*, 1992; Emery-Goodman *et al.*, 1993; Gray *et al.*, 1993; Philpott *et al.*, 1993; Hirling *et al.*, 1994). The RNA-binding and enzyme activities are mutually exclusive, and only the apo-protein conformation of IRP-1 permits access of the IRE to its RNA-binding surface. Thus, when cysteines anchoring the iron–sulfur cluster are mutated to serines, IRP-1 becomes constitutive for IRE binding (Philpott *et al.*, 1993; Hirling *et al.*, 1994). Yet, the IRE-binding site does not consist of a modular domain and requires a full-sized IRP-1 (Hirling *et al.*, 1992). IRP-1 shows sequence homology to mitochondrial aconitase and is presumably similarly folded with a centrally located active-site cleft and conserved substrate-binding residues (Robbins and Stout, 1989; Rouault *et al.*, 1991) (Figure 1).

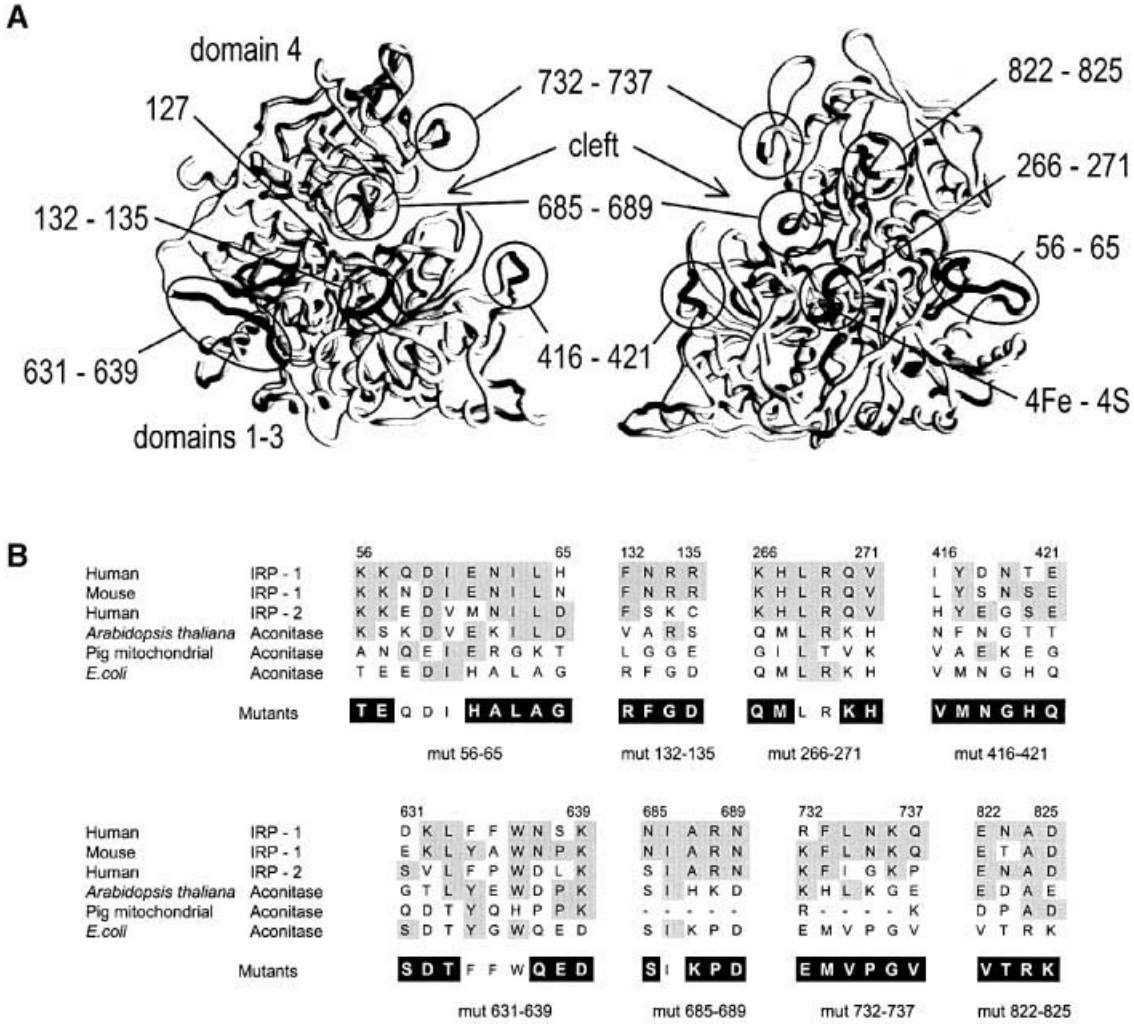

Fig. 1. Mutagenesis of predicted surface regions in IRP-1. Based on extensive sequence homology (Rouault *et al.*, 1990; Hirling *et al.*, 1992), the folding of human IRP-1 is assumed to resemble that of porcine mitochondrial aconitase (Rouault *et al.*, 1991), the structure of which is shown in (**A**) (Robbins and Stout, 1989; two views differing by an angle of 120° around a vertical axis). This permits the prediction of homologous IRP-1 sequences at the protein surface. For mutagenesis (circled areas), we selected surface regions or protruding loops, in and near the cleft between domains 1–3 and domain 4, which are conserved in IRP-1 and IRP-2, but distinct in aconitases without IRE binding. A sequence alignment of these regions is shown in (**B**) and includes human IRP-1 (Rouault *et al.*, 1990; Hirling *et al.*, 1992), mouse IRP-1 (Philpott *et al.*, 1991), human IRP-2 (Rouault *et al.*, 1992), plant aconitase of *Arabidopsis thaliana* (Peyret *et al*., 1995), porcine mitochondrial aconitase (Zheng *et al.*, 1990) and bacterial aconitase of *E.coli* (AcnA) (Prodromou *et al.*, 1992). Since only IRP-1 and IRP-2, but not bacterial aconitase, bind to human ferritin IREs, IRP-1 was mutagenized to the corresponding sequence of bacterial aconitase.

The N-terminal globular protein domains 1–3 of ~65 kDa contain the [4Fe–4S]-cluster at the surface of the substrate-binding cleft. These domains are connected by a hinge region to the C-terminal globular 30 kDa domain (domain 4) opposite the cleft. The substrate contacts both the [4Fe–4S]-cluster and domain 4 (Beinert *et al.*, 1996). It was proposed that the cleft should open in the apo-protein due to the flexibility of the hinge region, and thereby new contact sites for the IRE might become exposed (Klausner *et al.*, 1993). This view seems to be supported by several findings. First, alkylation of Cys437, which is deeply in the cleft of the holo-protein and holds the [4Fe–4S]-cluster, prevents binding of the IRE (Philpott *et al.*, 1993; Hirling *et al.*, 1994). Secondly, cross-linking with UV light of IRP-1 to a radioactive IRE labels the protein at residues 121–130, presumably at Ser127, which is predicted to reside near the cluster-binding Cys437 (Basilion *et al.*, 1994b). Without an opening of the cleft, neither Ser127 nor Cys437 would be accessible to an IRE, which has a larger diameter than the closed cleft (Laing and Hall, 1996; Addess *et al.*, 1997; Gdaniec *et al.*, 1998). Thirdly, mutations at conserved substrate-binding residues in the cleft were reported to affect the IRE binding of IRP-1 (Philpott *et al.*, 1994).

In addition, a second protein (IRP-2) with strong homology to IRP-1 and a similarly high affinity for IREs has been characterized in rodents, rabbit and man (Henderson *et al.*, 1993; Guo *et al.*, 1994; Samaniego *et al.*, 1994). This high-degree conservation in RNA binding and specificity (Henderson *et al.*, 1994, 1996) suggests that the amino acid sequence contacting the IRE is similar between IRPs. Yet, certain mutations in the IRE loop and bulge regions show rather exclusive binding to either IRP-1 or IRP-2 (Henderson *et al.*, 1994, 1996).

In the present study we identify two sites in domain 4 of IRP-1 that are important for IRE binding. For this we employed selective mutagenesis of surface areas that were predicted from the alignment of IRP-1 with IRP-2 and

aconitases of different origins as well as the crystal structure of porcine mitochondrial aconitase (Robbins and Stout, 1989; Rouault *et al.*, 1991, 1992). Whereas IRE–IRP-1 complex formation is readily measured in a gel-retardation assay, no RNA binding has been detected for mitochondrial (Kennedy *et al.*, 1992) or bacterial aconitases (Rothenberger *et al.*, 1990). Thus, there exist specific differences between IRP-1, IRP-2 and the other aconitases, which determine the RNA-binding properties. Based on this analysis, the human IRP-1 sequence was mutated in selected regions to resemble the corresponding counterpart of bacterial aconitase (Prodromou *et al.*, 1992). All mutants were expressed as recombinant proteins fused to a glutathione *S*-transferase (GST) domain, purified, and tested with respect to their IRE-binding activity. In order to ascertain the conformational integrity of the mutants, we also measured their aconitase activity. The newly identified RNA-binding sites of IRP-1 were confirmed in studying the binding of appropriate IRP-1/IRP-2 hybrid proteins to IRP-1-specific IREs.

Results

Sequence and structure comparison between aconitases and mutagenesis of IRP-1

IRP-1 and mitochondrial aconitase share all active-site residues of aconitases and show sufficient sequence homology to foresee that their structures must be closely related (Rouault *et al.*, 1991). Therefore, based on the crystal structure of porcine mitochondrial aconitase (Robbins and Stout, 1989) and sequence alignments, we predicted which regions of IRP-1 should be exposed at the surface (Figure 1). In order to identify potential IRE-binding sites, particular attention was paid to predicted surface regions within or near the cleft (Figure 1), as they might become exposed in the iron-deprived protein when the [4Fe–4S]-cluster and substrate are missing (Rouault *et al.*, 1991; Haile *et al.*, 1992; Kennedy *et al.*, 1992; Emery-Goodman *et al.*, 1993; Schalinske *et al.*, 1997). Such sites should be conserved in all IRE-binding proteins, notably IRP-1 and IRP-2 of various species, but absent in other members of the aconitase family from mitochondria, bacteria and plants (Rothenberger *et al.*, 1990; Frishman and Hentze, 1996). IRP-1 sequences of four mammalian species (human, rat, rabbit and mouse) (Rouault *et al.*, 1990; Philpott *et al.*, 1991; Hirling *et al.*, 1992; Patino and Walden, 1992; Yu *et al.*, 1992) show >90% identity. They are highly related to mammalian IRP-2 (Rouault *et al.*, 1992; Guo *et al.*, 1995; 62% identity and 80% similarity) and, more surprisingly, to plant cytoplasmic aconitases, such as that of *Arabidopsis thaliana* (Peyret *et al.*, 1995; 59% identity and 71% similarity), and to bacterial aconitase (AcnA) (Prodromou *et al.*, 1992; 52% identity), whereas the identity is lower with mammalian mitochondrial aconitase (Zheng *et al.*, 1990; 29% identity). While comparing known mitochondrial aconitase surface sequences with those of human IRP-1 and all other aconitase family members, it became evident that several regions were almost identical. We considered those to be less likely candidates for an IRP-specific RNA-binding site. Certain regions, however, were only conserved in mammalian IRP-1 and IRP-2, but differed markedly from the other sequences (Figure 1), a feature more compatible with a possible role in the IRE–IRP-1 interaction. Based on this analysis, we mutagenized eight predicted surface sequences of human IRP-1 to the corresponding sequence of bacterial aconitase (Figure 1) in order to test whether any of these alterations affected specifically IRE binding but not enzymatic function. In addition, a deletion mutant of amino acids 394–401 was constructed and analyzed.

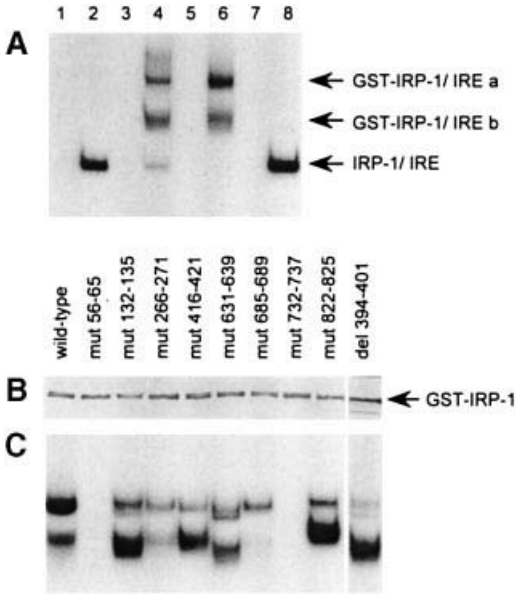

Fig. 2. Gel-retardation analysis with recombinant wild-type and mutant IRP-1. IRP-1 was expressed in bacteria with a GST-tag, affinity purified and analyzed for RNA binding with 0.2 ng of ^{32}P-labeled human H ferritin IRE (pSPT-fer; Müllner *et al.*, 1989). IRE–IRP complexes were resolved on a 6% non-denaturing polyacrylamide gel (**A**). Lane: 1, no protein; lane 2, human IRP-1 of 1 μg cytoplasmic extract of Jurkat cells; lane 3, extract of *E.coli* transformed with pGEX-2T vector alone; lane 4, extract of *E.coli* with full-length cDNA of human IRP-1; lane 5, efflux from glutathione–Sepharose with a bacterial control extract; lane 6, as in lane 5, but with recombinant IRP-1; lane 7, thrombin-cleaved control efflux; lane 8, thrombin-cleaved sample with recombinant IRP-1. GST-tagged IRP-1 mutants (10 ng) were analyzed by the same gel-retardation assay (**C**). To verify that similar amounts of recombinant IRP-1 were used in the assay, we analyzed 300 ng of each affinity-purified IRP-1 on a Western blot (**B**) with an anti-peptide antibody against amino acids 670–683 (Henderson *et al.*, 1993).

IRP-1 mutants were expressed in bacteria as recombinant hybrid proteins with an N-terminal 26-kDa GST-tag and a thrombin cleavage site. Upon incubation with a ^{32}P-labeled ferritin IRE, recombinant wild-type IRP-1 with the tag showed a triple band-shift, or a double band-shift after purification on a glutathione–Sepharose column (Figure 2A). The formation of all radioactive complexes was readily competed with excess unlabeled IRE (not shown). After cleavage of the tagged IRP-1 with thrombin, all complexes migrated at the same position as native human IRP-1 (Figure 2A). We conclude that the upper two bands correspond to complexes of the IRE with tagged IRP-1, whereas the lower band is a complex with processed IRP-1, some of which is present spontaneously in bacterial extracts and does not bind to glutathione–Sepharose. The GST-tagged IRP-1 tended to aggregate and produced variable amounts of the slowly migrating complex ‘a’ that we identified as dimers by gel chromatography (not shown). Analysis of fractions with aggregated

Table I. Aconitase activity of wild-type and mutant IRP-1

IRP-1	K_m (μM)	V_{max} (nmol/s/μg IRP-1)
wild-type	21	0.128
mut 56–65	na[a]	na
mut 132–135	20	0.125
mut 266–271	14	0.126
del 394–401	21	0.151
mut 416–421	20	0.153
mut 631–639	308	1.558
mut 685–689	23	0.152
mut 732–737	179	0.371
mut 822–825	15	0.052
mut 732A	185	0.440
mut 732B	271	0.420
mut 732C	38	0.157
mut 732D	153	0.498
mut 732E	64	0.317

[a]na, no activity detected.
Freshly isolated recombinant IRP-1 (10 μg) was analyzed immediately for aconitase activity with different concentrations of *cis*-aconitate. The consumption of substrate was monitored at 240 nm. Data were registered every 12 s and analyzed by linear regression in a Lineweaver–Burke plot. The data were reproducible in two experiments with a standard deviation of the linear regression of ~10%.

or processed wild-type IRP-1 indicated no difference in affinity for the IRE (not shown). Thus, GST-tagged IRP-1 is equally informative for a qualitative and quantitative assessment of RNA binding.

Functional tests of mutant IRPs indicate specific binding sites

Each mutant was submitted to measurement of its interaction with the ^{32}P-labeled ferritin IRE and an independent determination of its aconitase activity. This latter control was introduced to ascertain that the IRP structure was not altered extensively by the mutagenesis. By varying the initial substrate concentration, the K_m and V_{max} were determined. As shown in Table I, all except mut 56–65 consistently showed aconitase activity, although we noticed changed K_m and V_{max} values in some of them. When iron–sulfur loading of the recombinant aconitases was boosted by the *in vitro* insertion of a [4Fe–4S]-cluster (Emery-Goodman *et al.*, 1993), V_{max} values did not usually increase much, suggesting that most of the freshly isolated recombinant IRP-1 was already in its iron-loaded aconitase conformation. The data show that mut 56–65 may have an aberrant folding.

Figure 2C depicts the RNA–protein gel-retardation assay obtained with fresh extracts of GST-tagged recombinant wild-type and mutant IRP-1. Mut 56–65 and mut 732–737 were strongly affected in their IRE-binding properties, whereas some others, e.g. mut 266–271 and mut 685–689, seemed to be partially affected. In order to achieve a more quantitative assessment, we assayed thrombin-digested mutant IRP-1 at different dilutions in the presence of a constant amount of ^{32}P-labeled ferritin IRE (Figure 3). Approximately 1.5 ng of wild-type IRP-1 was sufficient to shift half of the radioactive probe, whereas a several-fold greater amount of certain mutant IRPs was required, suggesting an accordingly lower affinity (Table II). This was notably the case for mut 56–65, which showed a 20-fold lower binding than wild-type IRP-1, and for mut 732–737, which was affected up to 7-fold, whereas mut 685–689 showed a 2.5-fold lower affinity. All other mutants showed as strong IRE binding as wild-type IRP-1, and their mutations can be considered outside the critical region of the RNA–protein interaction.

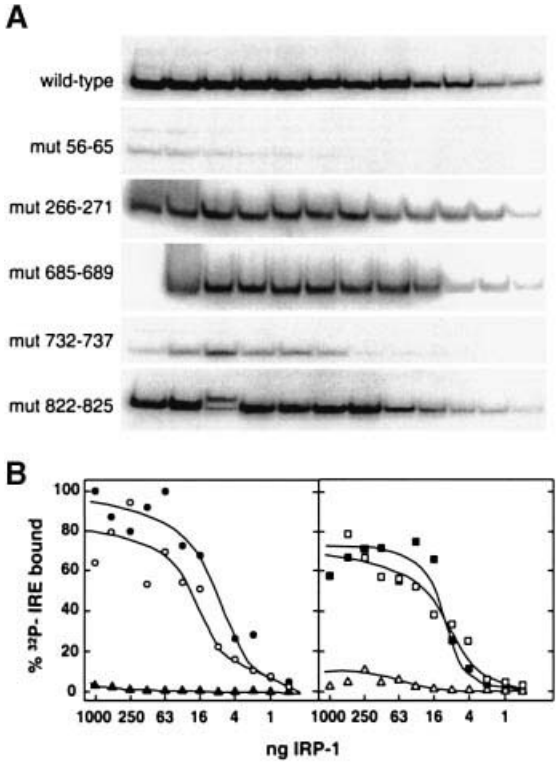

Fig. 3. Quantification of wild-type and mutant IRP-1 binding to an IRE by gel-retardation assay. Doubling dilutions of recombinant IRP-1 were incubated with a constant amount of IRE probe. (**A**) Representative band-shifts are shown for samples of wild-type IRP-1 and five IRP mutants. (**B**) The RNA–protein interaction was quantified with the PhosphorImager. These data were used directly for calculations of relative binding efficiency reported in Table II. The percentage bound IRE is shown for wild-type IRP-1 (●), mut 56–65 (▲), mut 266–271 (○), mut 685–689 (□), mut 732–737 (△) and mut 822–825 (■). The initial concentration corresponded to 1 μg IRP-1.

Table II. Relative affinities of mutant IRP-1 for human ferritin IRE

IRP-1	Relative binding efficiency	Mean ± SD
wild-type	1.00	1.00
mut 56–65	0.04; 0.05; 0.07; 0.04	0.05 ± 0.02
mut 132–135	0.79; 2.0	1.39 ± 0.86
mut 266–271	0.99; 0.99	0.99
del 394–401	1.02; 0.82	0.92 ± 0.15
mut 416–421	0.94; 0.40; 0.80	0.72 ± 0.28
mut 631–639	0.97; 0.70; 0.88	0.85 ± 0.14
mut 685–689	0.55; 0.23; 0.31; 0.78; 0.27	0.43 ± 0.23
mut 732–737	0.14; 0.17; 0.14; 0.18; 0.27; 0.23; 0.27	0.20 ± 0.06
mut 822–825	0.60; 1.18	0.89 ± 0.41

Recombinant wild-type and mutant IRP-1 were purified, cleaved from the GST-tag with thrombin and analyzed at different dilutions in gel-retardation assays (Figure 3A). Autoradiograms of shifted RNA–protein complexes were quantified by the PhosphorImager, and bound radioactivity plotted as a function of recombinant protein concentration (Figure 3B). The amount of IRP-1 that achieves half-maximal binding of a ferritin IRE was determined in independent isolates, and the values were normalized in each experimental series to those of wild-type IRP-1, which was arbitrarily set at 1.

All affected mutants were carefully re-analyzed by a more refined quantitative filter method, which we introduced to assess the affinity of IRE–IRP interactions. A constant amount of fresh GST-tagged recombinant IRP-1 was incubated with increasing amounts of IRE, of which a fixed quantity was radioactively labeled. Complexes were then separated from unbound IRE by filtration through 0.1 μm Millipore filters. We found that complexes were well retained on such filters, whereas the unbound IRE was not (for details, see Materials and methods). The retained radioactivity was quantified, and the affinity of the IRE–IRP interaction calculated by transformation of the values into Scatchard plots (Figure 4). The affinities between the wild-type IRE 42 and a selected set of mutant IRP-1 are reported in the upper left of Table III. In this assay we confirmed that mut 56–65, mut 685–689 and mut 732–737 were affected in their binding compared with the wild-type IRP-1.

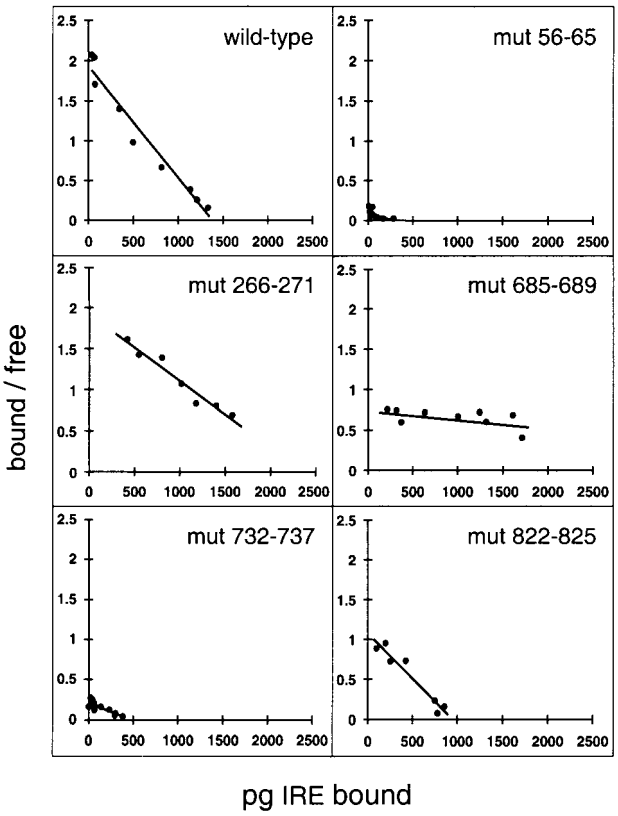

Fig. 4. Scatchard analysis of wild-type IRE binding to wild-type and mutant IRP-1. Affinity-purified GST-tagged wild-type and mutant IRP-1 were analyzed for their IRE-binding affinity at 23°C with 15 pg of ^{32}P-labeled IRE and increasing amounts of unlabeled IRE (0.5–6 ng). The bound IRE fraction was determined after filtration through 0.1 μm nitrocellulose filters. Radioactivity of complexes retained on the filter was quantified by autoradiography on a PhosphorImager screen. Data were transformed into Scatchard plots (Table III).

Importance of domain 4 of IRP-1 for IRE binding

Since mut 732–737 showed a clear difference compared with wild-type IRP-1 in the interaction with IREs, we analyzed this region further by introducing finer mutations affecting only one or a few amino acids (Figure 5). A triple mutation at amino acids 732, 733 and 736 (mut 732D) clearly affected the gel-retardation assay for IRE binding, whereas the complementary mutant with altered amino acids 734, 735 and 737 (mut 732E) gave a strong band-shift (Figure 5B). Further mutagenesis of the basic and aromatic residues in mut 732D, one by one, revealed that an Arg732→Glu mutation (mut 732A) caused some loss of binding, whereas amino acids 733 and 735 seemed less critical. This conclusion was clear-cut and reproducible with the filter assay and Scatchard plot analysis (Figure 5C). The calculated affinities of these mutants with the wild-type IRE 42 are reported in the lower left of Table III. We conclude that Arg732 is the most critical amino acid in this region for the IRE–IRP interaction. In control experiments, all the mutants showed a strong aconitase activity, although the K_m was slightly higher in several of them (Table I).

Direct interaction of domain 4 with the IRE loop and bulge

Previously we have demonstrated by the selex method that a restricted number of mutant IREs with altered loop or bulge sequences can still bind to IRP-1, generally with a 2- to 6-fold reduced affinity (Henderson *et al.*, 1994, 1996). These IRE mutants define the highly conserved loop and bulge nucleotides as critical determinants for the

Table III. Affinities of wild-type or mutant IRP-1 for different IREs

IRP-1	IRE 42 C.....CAGUGC	IRE 14 C.....CAAUGC	IRE 17 C.....GAGUGU	IRE 57 A.....CAGUGA
wild-type	4.5 ± 0.6 (4)	15.8 ± 6.5 (4)	3.9 ± 2.0 (4)	3.3 ± 0.1 (3)
mut 266–271	5.8 ± 1.0 (2)	n.d.	n.d.	n.d.
mut 685–689	12.5 ± 6.4 (4)	10.8 ± 1.0 (3)	19.3 ± 0.1 (3)	35.0 ± 4.1 (2)
mut 732–737	12.1 ± 3.4 (3)	33.7 ± 0.7 (2)	>100 (3)	37.2 ± 2.6 (3)
mut 822–825	5.0 ± 0.5 (2)	9.6 ± 4.5 (3)	2.6 ± 0.8 (4)	6.6 ± 1.1 (2)
mut 732A	12.5 ± 1.3 (3)	27.2 ± 13.2 (3)	23.2 ± 5.0 (4)	7.7 ± 1.8 (3)
mut 732B	2.6 ± 2.0 (2)	11.3 ± 4.3 (3)	10.5 ± 2.6 (3)	4.0 ± 1.2 (3)
mut 732C	4.4 ± 2.0 (4)	7.3 ± 0.6 (3)	20.9 ± 6.6 (3)	6.3 ± 0.3 (3)
mut 732D	13.7 ± 3.8 (3)	33.1 ± 10.8 (2)	210 ± 45.3 (2)	51.1 ± 7.0 (3)
mut 732E	4.4 ± 2.5 (3)	21.7 ± 3.8 (3)	23.8 ± 16.1 (3)	48.1 ± 4.9 (3)

Recombinant GST-tagged wild-type and mutant IRP-1 were purified on glutathione–Sepharose and analyzed by a filter assay (see Materials and methods) for the binding of different IREs. IRE 42 corresponds to a sequence almost identical with the wild-type ferritin IRE sequence, whereas IRE 14 is altered at loop position 3, IRE 17 at loop position 1 and IRE 57 in the bulge C residue (Henderson *et al.*, 1994). All K_d values reported are derived from Scatchard plots (like those in Figures 4 and 5) and have the dimension 10^{-10} M. The number of experiments is given in parentheses. n.d., not determined.

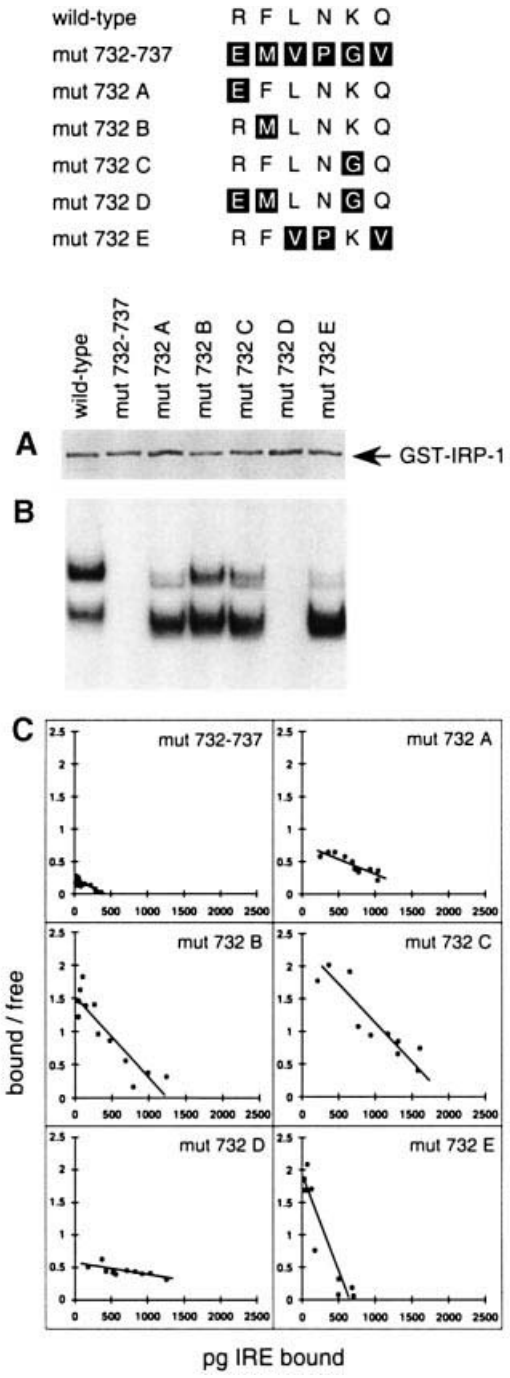

Fig. 5. Gel-retardation and Scatchard analysis of complexes between wild-type IRE and IRP-1 with mutations at amino acids 732–737. IRP-1 mutants were made by site-directed mutagenesis as listed. Recombinant protein (300 ng) was analyzed on a Western blot (**A**), and equal amounts of GST-tagged IRP-1 (10 ng) were incubated with 0.2 ng of human ferritin H chain IRE prior to the RNA–protein gel-retardation assay (**B**). For Scatchard analysis (**C**), 50 ng of GST-tagged recombinant wild-type or mutant IRP-1 were incubated for 10 min at 23°C with 15 pg of ^{32}P-labeled wild-type IRE and increasing amounts of unlabeled IRE (0.5–6 ng) in 50 µl of incubation buffer (see Materials and methods). IRE–IRP complexes were filtered through 0.1 µm nitrocellulose filters, and the radioactivity retained was quantified by autoradiography on a PhosphorImager screen. Data were transformed into Scatchard plots (Table III).

specificity of RNA recognition by IRP-1. To study whether IRP-1 mut 685–689 and mut 732–737, or submutants thereof, affect the interaction with the loop or the bulge, we tested their binding affinity for three IRE mutants. We chose to analyze IREs with a mutation in the first or third residue of the loop (IRE 17 and IRE 14, respectively) as well as an IRE with a C→A mutation in the bulge (IRE 57). We measured the affinities by the filter method for all possible combinations (Table III). Wild-type IRP-1 and mut 822–825 served as controls in this analysis.

The data confirm the importance of amino acids 685–689 and 732–737 in the IRE–IRP interaction. Mut 732–737 and submutants 732A and 732D were affected with all IRE probes, indicating again the significance of Arg732 for the IRE binding. Moreover, different affinities were observed with different IRE probes. For example, IRE 14 bound to most IRPs with a 2- to 3-fold lower affinity than the wild-type IRE 42. This suggests the existence of a critical contact site for the ^{3}G residue of the six-nucleotide CAGUGC loop sequence. A combination of effects was observed for all mutants at Arg732: the 2- to 3-fold weaker affinity for the wild-type IRE was affected a further 3-fold when IRE 14 was bound, and resulted in a 6- to 8-fold lower binding overall. These differences are best understood by the existence of multiple RNA–protein interaction sites: for example, mutations at two independent interaction sites, once on the IRE and once on the IRP-1, could explain the above results. Interestingly, mut 685–689 compared with the wild-type IRP-1 showed no further loosening of the interaction when incubated with IRE 14. On the contrary, it bound better than the wild-type IRE. In this case, the data suggest that no additional interaction site was affected. A stronger binding suggests that loop-nucleotide ^{3}G interacts either directly with one of the mutated amino acids 685–689 or some neighboring amino acids in domain 4 whose conformation is more favorable in this IRP-1 mutant. A multiple effect on the affinity was also observed between IRE 17 and all mutants in the region 732–737. Furthermore, the bulge mutant IRE 57 showed a low affinity with mut 685–689, and with IRP-1 mutants carrying multiple amino acid changes in region 732–737. However, surprisingly, mut 732A bound better to IRE 57 than to the wild-type IRE. This suggests that the C→A mutation in the bulge improves the fitting with the IRP-1 Arg732→Glu mutant, and this can be interpreted as a direct contact of the bulge with domain 4.

IRP-1-specific binding of IRE mutants requires certain amino acids in domain 4

In order to test whether the newly identified surface regions of domain 4 account for the specificity of IRP-1 binding to certain IRE mutants and whether they are sufficient for this binding, we made hybrid proteins between IRP-1 and IRP-2. Amino acids 685–740, 685–710 or 711–740 of human IRP-1 were replaced by the corresponding region of human IRP-2, and the hybrid proteins tested in gel-retardation assays (Figure 6A). They bound to the wild-type IRE 42 as strongly as non-modified IRP-1, indicating no major changes in their structure. However, the binding to IRP-1-specific IREs 25, 39, 3 and 35 (Henderson *et al.*, 1994), which carry specific modifications in their loop sequences, was lost when amino acids 685–710 in IRP-1 were replaced by those of IRP-2. This confirms the importance of this region for binding of the IRE loop. In contrast, binding of the

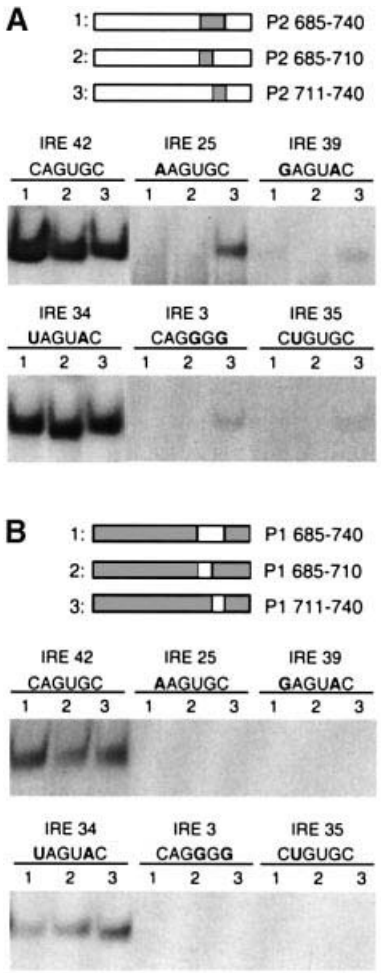

Fig. 6. Gel-retardation assays of IRP-1/IRP-2 hybrid proteins with IRP-1-specific IREs. In (**A**) three different constructs (lanes 1–3) of hIRP-1 with short replacements at amino acids 685–740, 685–710 or 711–740 by corresponding IRP-2 sequences (top drawing) were incubated with either the wild-type IRE 42 or IRP-1-specific IREs 25, 39, 34, 3 and 35 (Henderson *et al.*, 1994). Mutations present in the loop sequences of these IREs are indicated above the lanes. The hybrid proteins had no GST-tag. Protein and probe concentrations were chosen such that half the wild-type IRE 42 probe was shifted. In (**B**) reverse protein constructs with an IRP-2 backbone and IRP-1 insertions were assayed for binding to the same IREs.

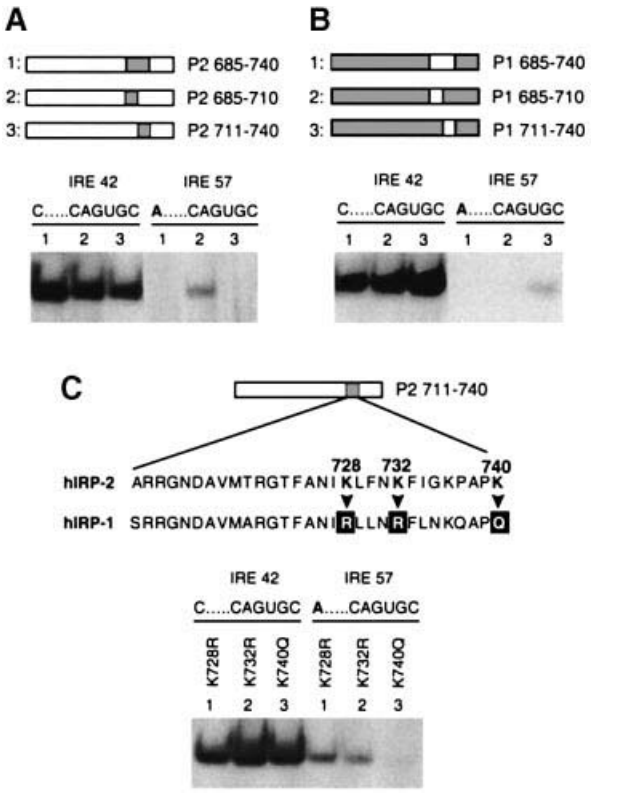

Fig. 7. Assays of IRP-1/IRP-2 hybrid proteins with the IRP-1-specific IRE 57 that has a mutation in the bulge. In (**A** and **B**), the same protein constructs as in Figure 6 were assayed for binding to IRE 57, which has an unpaired adenine instead of a cytosine immediately 5′ of the upper IRE stem. In (**C**), we analyzed additional mutants of IRP-1($P2_{711–740}$) in which single lysines of the IRP2 insert were mutated back to the amino acid of IRP-1 at this position.

IRP-1-specific IREs was preserved when amino acids 711–740 were replaced. The signal was weaker than with a wild-type IRE. This is expected since IRE mutants also show a weaker binding to wild-type IRP-1 (Henderson *et al.*, 1994). IRE 34, like the wild-type IRE, was not sensitive to these IRP-1 modifications. The mutated nucleotides in loop positions 1 and 5 of IRE 34 interact with each other (Henderson *et al.*, 1994; Laing and Hall, 1996; Addess *et al.*, 1997; Gdaniec *et al.*, 1998) and might be more important for IRE structure than the contact with domain 4. In the reverse constructs (Figure 6B), grafting of human IRP-1 amino acids 685–740 into human IRP-2 was not sufficient to confer IRP-1-specific IRE binding. This suggests that residues outside this region also contribute to the recognition of the loop. We also did not observe IRP-2-specific IRE binding with the hybrid constructs (data not shown). Since IRP-2-specific IREs bind very weakly to wild-type IRP-2 (Henderson *et al.*, 1996), a failure to detect their binding to hybrid proteins might be due to detection limits and/or dissociation of complexes during gel migration.

The same constructs were also tested with the IRP-1-specific IRE 57 that has the C→A mutation in the bulge. Gel-retardation assays show loss of IRE 57 binding when the region 711–740 of IRP-1 is replaced by the sequence of IRP-2, but no change with a replacement at 685–710 (Figure 7A). Grafting the IRP-1 region 711–740 into IRP-2 confers IRP-1-specific binding to IRE 57 to IRP-2 (Figure 7B), which itself does not bind this IRE (Henderson *et al.*, 1994). Thus, this region appears to be necessary and sufficient for the recognition of an A-bulge. Since human IRP-1 and IRP-2 differ only slightly at 711–740, we tried to identify important amino acids present in IRP-1 but missing in the IRP-1($P2_{711–740}$) mutant. Three lysines in the human IRP-2 sequence of this hybrid protein were mutated back to the residues present in IRP-1. The Lys728→Arg, Lys732→Arg and to a much lesser extent the Lys740→Gln mutations of IRP-1($P2_{711–740}$) restored the IRP-1-specific binding to IRE 57 (compare Figure 7C with A, last lane). This indicates that arginines 728 and 732 are critical for the interaction of IRP-1 with the unpaired base of the IRE bulge.

Discussion

The results of the present study newly attribute the IRE hairpin-binding properties of IRPs to protruding surface

loops in their domain 4. As IRPs neither belong to any classical RNA-binding protein family nor consist of modular domains, no obvious predictions about IRE-binding surfaces could be made. We therefore took an approach of site-directed mutagenesis in order to identify regions required for the interaction. Given the size of the protein, we restricted the search to IRP surfaces inside or near the active-site cleft (Figure 1) and selected for mutagenesis unique sequence patterns mostly shared between IRP-1 and IRP-2 but absent from other members of the aconitase protein family.

We identified three regions in human IRP-1 that affect the binding of IREs: two in domain 4, encompassing amino acids 685–689 and 732–737, and one in domain 1, at amino acids 56–65. The two domain 4 mutants retain good aconitase activity when loaded with an [4Fe–4S]-cluster and are, therefore, correctly folded. However, mut 56–65 was absolutely inactive both in RNA-binding and aconitase activity. This suggests that the latter mutation prevents either the insertion of the [4Fe–4S]-cluster or the substrate binding and transformation. Yet, based on the structure of mitochondrial aconitase (Robbins and Stout, 1989), the altered region in mut 56–65 does not contain any active-site residues that interact directly with citrate. The model (Figure 1) predicts that these amino acids reside at the surface, rather than in the active center. We cannot distinguish, therefore, whether the dramatic simultaneous changes in activities reflect a misfolding of IRP-1 or are the consequence of a mutation in authentic RNA-binding residues.

In contrast, the two mutants in domain 4 seem to affect exclusively a local area predicted as the surface at the edge of the cleft. A closer look at the alignment with other aconitases reveals that the two mutated regions of IRP-1 show quite good homology with IRP-2. Although the sequences diverge from bacterial and plant cytoplasmic aconitases, IRP-1 shares with them a similarly sized stretch of amino acids between adjacent blocks of strong homology. However, both the 685–689 and 732–737 regions lie in areas where the sequences of all mitochondrial aconitases are considerably shorter. IRP-1 685–689 is part of a 9-amino-acid stretch that is missing in pig mitochondrial aconitase between positions 574 and 575, while IRP-1 732–737 corresponds to a 5-amino-acid gap between positions 600 and 601 in the mitochondrial protein. As a consequence, the corresponding surface loops in IRP-1 are expected to be larger and to protrude further towards domains 1–3 than in mitochondrial aconitase. Considering the evolutionary relationship between prokaryotic and eukaryotic aconitases, it seems likely that in animals the RNA-binding property was gained in part from minor modifications in some exposed loops. Not all protruding loops were recruited for RNA binding as the deletion between amino acids 394 and 402, which encompasses an additional surface loop in IRP-1, showed no effects on IRE binding (and aconitase activity). The other mutations, which had no effect on the IRE–IRP interaction, lie in regions where the amino acid sequence of mitochondrial aconitase is not shorter than IRP-1.

None of our present mutants overlap with previously mapped aconitase active-site residues, as we did not consider highly conserved areas in our mutagenesis scheme. However, a previous study has implicated several substrate-coordinating arginines in IRE binding, notably residues 536, 541 and 780, but not 699 (Philpott *et al.*, 1994). A conceptual problem exists with these mutants. By definition, they affect conserved active-site residues and aconitase activity, i.e. amino acids which are located in central positions and are probably critical for correct protein folding. To verify the integrity of the mutated IRP-1, it would seem necessary to have an independent criterion to assess the IRP structure. In the case of the active-site arginine mutants, there is unfortunately none. Similarly, in our mut 56–65 it is not possible to decide whether these residues are really involved in the RNA binding or whether the protein is merely misfolded, even if its electrophoretic migration seems normal. However, the presence of aconitase activity in the absence of IRE binding represents an independent control for folding.

Our study shows that domain 4 cooperates with domains 1–3 in binding the IRE. A requirement of domain 4 in IRE binding was already postulated by us based on C-terminal deletion mutants (Hirling *et al.*, 1992). Moreover, an IRE–IRP cross-link site by UV light maps to domain 1 of human IRP-1 (Basilion *et al.*, 1994b; Neupert *et al.*, 1995) between amino acids 121 and 130, presumably at Ser127 (Basilion *et al.*, 1994b). In addition, mutagenesis of IRP-1 Cys437, which ligates the [4Fe–4S]-cluster, revealed that reduction of this residue is critical for the IRE–protein interaction (Philpott *et al.*, 1993, 1994; Hirling *et al.*, 1994).

Taken together, the data clearly indicate multiple RNA–protein interaction sites at the cleft. This is further supported by the affinity measurements with IRE mutants. They show no complete loss of binding, but rather a combinatorial loosening of the interaction when tested against mutant IRPs (Table III). Up to now, the actual structures of IRP which contact the IRE still cannot be predicted as no known crystal coordinates exist for the loops which comprise sequences 685–689 and 732–737. Nonetheless, based on two independent lines of evidence, we can conclude that Arg728 and Arg732 are necessary and probably sufficient for contact of IRP-1 with the unpaired nucleotide in the IRE bulge. Mutagenesis of Arg732 in IRP-1 lowers the affinity for a wild-type IRE considerably (Table III), and IRP-1-specific IRE binding is only observed when either arginine is present in IRP-1/IRP-2 hybrid proteins (Figure 7). We also provide evidence that the IRP-1 region comprising residues 685–689 is required but not sufficient for contacts with bases in the IRE loop. In addition, this region contains an arginine that is conserved in IRPs but not present in bacterial aconitases. Further experiments are needed to decide whether this residue is involved in binding. While basic residues may mediate initial charge interactions with the RNA, arginines are also frequently involved in hydrogen bonding with the sugar backbone or specific bases (Burd and Dreyfuss, 1994). Direct recognition of bases by IRPs must indeed occur, as both IRE loop and bulge nucleotides confer specificity to the binding (Henderson *et al.*, 1994, 1996). This is supported by the NMR structure of a wild-type IRE (Laing and Hall, 1996; Addess *et al.*, 1997; Gdaniec *et al.*, 1998) and by recent chemical probing of IRP contact sites on the IRE (Schlegl *et al.*, 1997). These studies indicate that there is a preferred IRE surface comprising the loop and the bulge C, which is protected

from chemical modification by binding of IRP-1. We propose that the loop, and in particular the G-residue in position 3 (Table III), is in close contact with the region 685–689, and that the bulge C interacts with the region of Arg728 and Arg732. Such a model is compatible with steric considerations. The distance of 25 Å between the bulge C and the loop G in a wild-type IRE (Addess *et al.*, 1997) corresponds closely to the distance of 22.5 min Å estimated between amino acids 574/575 and 600/601 in the mitochondrial aconitase crystal. These amino acids represent the insertion site for the additional protruding loops of IRP-1.

If we project the hitherto identified IRE contact sites onto the mitochondrial aconitase structure, it appears that the RNA is most likely to bind at the cleft of IRP-1 (Figure 1). The variable opening of this cleft was proposed as the mechanism by which the enzymatic and RNA-binding functions of IRP-1 become mutually exclusive (Klausner *et al.*, 1993). In the enzymatic closed conformation, the IRE-binding sites would remain inaccessible and only open after [4Fe–4S]-cluster and/or substrate removal. Probably the strongest argument in favor of the postulated conformational change is the modulation of protein phosphorylation or protease accessibility in the absence of such a cluster (Schalinske *et al.*, 1997), and the position of the RNA–protein cross-link site, Ser127 (Basilion *et al.*, 1994a), which resides in the cleft near the [4Fe–4S]-cluster. This site cannot be touched by the IRE hairpin without an opening, because the diameter of a double-stranded RNA hairpin is much larger (Laing and Hall, 1996; Addess *et al.*, 1997; Gdaniec *et al.*, 1998) than the closed cleft. The results obtained with our new mutants are perfectly in line with this idea although they do not *per se* prove or disprove the opening of the cleft, as the newly identified contact sites are situated rather at the outer edge of the cleft in domain 4. The present data favor the view of an RNA-binding conformation that would permit simultaneous binding to the IRE loop and bulge near amino acids 685–689 and at Arg728, Arg732, respectively, with an additional interaction of the IRE, perhaps by its opposite surface, at the cross-link site, Ser127. We conclude that cytoplasmic aconitase in animals acquired a peculiar type of RNA binding, which requires simultaneously widely separate protein domains, and this provides important clues for a coherent model of the IRE–IRP interaction, whose elucidation has remained unsuccessful hitherto (Addess *et al.*, 1997). The present results will gain further interest once precise modeling of the IRE–IRP interaction is accessible. This will require the co-crystal structure of an IRE–IRP complex or at least the coordinates of the surface residues in domain 4 of IRP-1.

Materials and methods

Vectors for IRP-1 expression and site-directed mutants

The full-length cDNA coding for human IRP-1 (Hirling *et al.*, 1992) was subcloned into the bacterial expression vector pGEX-2T (Smith and Johnson, 1988) (Pharmacia, Uppsala, Sweden) in-frame behind the coding region of the 26 kDa fragment of GST under the control of the IPTG-inducible tac-promoter. The new plasmid is called pGEX-hIRP. Site-directed mutagenesis was performed by the method of Kunkel *et al.*, (1987) as described previously by using single-stranded DNA derived from pGEM-hIRP as a template (Hirling *et al.*, 1994). For mutagenesis between amino acids 1 and 758, a cDNA lacking its 3′-terminal *Kpn*I fragment was mutated, whereas sequences encoding the C-terminal end were mutated with the subcloned *Kpn*I fragment (from position 2384 to the 3′-end). Oligonucleotides with specific mismatches were hybridized to the single-stranded DNA, and the second strand synthesized with 1 U T4 DNA polymerase (Boehringer Mannheim, Germany) in the presence of 0.5 mM dATP, dCTP, dGTP and dTTP, 3 mM $MgCl_2$, 50 mM NaCl, 20 mM Tris–HCl pH 7.6, 2 mM dithiothreitol, 1 mM ATP and 3 U T4 DNA ligase (Boehringer). Double-stranded DNA was transformed into BZ234 bacteria and mutants selected by sequencing (Sanger *et al.*, 1977). Mutant DNA fragments were reassembled in the pGEX-hIRP expression vector and verified by resequencing. The oligonucleotides for mutagenesis were complementary to the coding strand and had the following sequences: mut 56–65, AGTGACATTCCAA**CC**T**GC**-AA**GGGC**A**TG**AATATCCTGTT**CC**G**T**CACCAAAAACTCATC; mut 132–135, GTAAACTGTCTGC**ATCG**C**C**G**AAG**C**G**ATCAACCTGG-AT; mut 266–271, ACTACCCCA**TGT**T**T**GCGGAG**CAT**CT**G**GGTAA-TGGT; mut 416–421, AGGGTGAATT**GA**T**GG**C**CG**T**TCAT**GA**C**-AAAGGTCTTATG; mut 631–639, GATATACGTAGAA**TCTTCCT**GC-CAGAAAAAC**GTATCAC**TTGATGGGGTTGC; mut 685–689, AGCA-GCAGGACTGT**CT**G**G**T**T**AATA**C**TTCCAGCTGGGG; mut 732–737, CTGTGGTGCC**ACACCTGGA**A**CC**A**TTTC**GTTTAACAAGC; mut 822–825, TGAGCCCCAGGGC**TTTACGGG**TC**A**CACCAGGGAGA-TAT. Sub-mutants 732A–E were also obtained by mutagenesis of wild-type IRP-1 with the following oligonucleotides: mut 732A, CTTGTTCA-AAAAT**TC**GTTTAACAAGC; mut 732B, CTGCTTGTTCAA**CA**T**T**-CTGTTTAACAA; mut 732C, CTGTGGTGCCTG**ACC**GTTCAA-AAATCT; mut 732D, AGTCTGTGGTGCCTG**ACC**GTTCAA**CA**T**TT**-**C**GTTTAA; mut 732E, CTGTGGTGCC**AC**CTT**TGGA**A**C**AAAT-CTGTTTAACAAGC.

The deletion mutant 394–401 was made from a subcloned *Bam*HI–*Eco*RV fragment (position 143–1871). The insert was cut at unique sites for *Sty*I (1283) and *Eco*RI (1368), filled in and religated by blunt-end ligation. The resulting clone was recut at the conserved *Eco*RI (1368) and unique *Bst*EII sites (1538). The excised fragment was replaced by the *Hin*fI–*Bst*EII fragment (1309–1538), again using blunt ligation after filling the *Eco*RI and *Hin*fI sites. The product results in the translated sequence ^{393}Leu-Glu-Leu-^{402}Phe at the deleted position.

Vectors for IRP-1/IRP-2 hybrid proteins

The cDNAs of human IRP-1 (Hirling *et al.*, 1994) and IRP-2 (Samaniego *et al.*, 1994) were PCR amplified and subcloned between the *Sal*I and *Not*I sites of pGEX 5X-3 (Pharmacia) in-frame behind the coding region of the GST-tag. Hybrid cDNAs were constructed from fragments of IRP-1 and IRP-2 by successive PCR amplification with oligonucleotides overlapping the joints. The constructs are designated IRP-1($P2_{x–y}$) to indicate that amino acids x–y of human IRP-2 were inserted into human IRP-1. An analogous nomenclature is used for the reverse constructs. IRP-1($P2_{711–740}$) was mutagenized to convert lysines 728, 732 or 740 of IRP-2 to the corresponding amino acids in IRP-1. This was achieved by PCR amplification using oligonucleotides with appropriate mutations.

Purification of IRP

For expression, plasmids were transformed into HB101, and bacteria grown in 2× YT at 37°C to OD_{600} 0.6 prior to overnight induction with 0.1 mM IPTG at 26°C. Proteins were extracted from bacteria in PBS, 1% Triton X-100 by a 40 s sonication on ice with a Branson sonicator at position 2. The extract was centrifuged for 30 min at 12 000 *g* and recombinant IRP in the supernatant adsorbed on 600 µl of glutathione–Sepharose (Pharmacia) by slow rotation at 4°C for 1 h. Beads were loaded onto a small column, washed with 6 ml of lysis buffer and 6 ml of PBS. The fusion-protein was eluted with 5 mM reduced glutathione in 50 mM Tris–HCl pH 8. Alternatively, IRP-1/IRP-2 hybrid proteins were recovered by cleaving the GST-tag with 0.06 U Factor Xa (Pharmacia)/0.5 ml PBS. Yields were 50–200 µg IRP per liter of culture. For measurements of aconitase activity, samples were freshly made and kept on ice. Purified IRP-1 was quantified by the Bio-Rad protein assay and its quality assessed by SDS–PAGE and Coomassie Blue staining.

Western blot analysis

IRP-1 was transferred from SDS–polyacrylamide gels to nitrocellulose filters. Western blots were incubated with rabbit anti-human IRP-1 serum (dilution 1:500) against the peptide 670–683: NLGDSVTTDHISPA (Henderson *et al.*, 1993). For the color reaction, alkaline phosphatase-conjugated second antibody and reagents of the ProtoBlot kit (Promega, Madison, WI) were used.

In vitro transcription of IREs

Plasmids used for *in vitro* transcription were either pSPT-fer containing the human ferritin H-chain IRE (Müllner *et al.*, 1989), or plasmids (Henderson *et al.*, 1994, 1996) containing the wild-type IRE (IRE 42) or mutated sequences: IRE 3 (loop CAG**GG**G), IRE 14 (loop CA**A**UGU), IRE 17 (loop **G**AGUGU), IRE 25 (loop **A**AGUGC), IRE 34 (loop **U**AGU**A**C), IRE 35 (loop C**U**GUGU), IRE 39 (loop **G**AGU**A**C) or IRE 57 (with an A in the bulge instead of a C). All plasmids were linearized with *Bam*HI prior to transcription. Radiolabeled IREs were transcribed in the presence of 1.5 mM ATP, UTP and GTP and 50 µCi [α-^{32}P]CTP (800 Ci/mmol) (Amersham Corp.) to yield a probe with a specific activity of 1.3×10^6 d.p.m./ng RNA. The radiolabeled IRE was purified on a denaturing 15% polyacrylamide gel. Unlabeled transcripts were purified on 3% NuSieve agarose gels (FMC Corp., Rockland, ME) as described previously (Henderson *et al.*, 1993) and quantified at 260 nm by comparison with a tRNA standard.

Gel-retardation assay

Gel-retardation assays were performed with a ^{32}P-labeled IRE as described previously (Rothenberger *et al.*, 1990). For IRP-1 mutants, assays were carried out with either GST-tagged recombinant protein or after thrombin cleavage of the tag. For this, 2.5 µg of freshly purified recombinant IRP-1 were digested for 1 h at 37°C with 0.25 µg thrombin from bovine plasma (Sigma T7513) in a total 35 µl of 50 mM Tris–HCl pH 8, 5 mM glutathione. To determine the protein concentration, which binds 50% of 0.3 ng IRE probe (2×10^5 c.p.m.), the highest IRP-1 concentration was adjusted to 1 µg recombinant protein/20 µl assay volume. Serial 1:2 dilutions were made thereof in 0.02% bovine serum albumin. All IRP-1 samples were fully activated by 2% 2-mercaptoethanol prior to the analysis (Hentze *et al.*, 1989). Recombinant cleaved IRP-1/IRP-2 hybrid proteins were analyzed at a concentration that shifts 3×10^4 c.p.m. wild-type IRE probe half-maximally. Only with hybrid proteins, 2.5 mg/ml heparin was added after the binding reaction. Autoradiograms were quantified using a Compaq PhosphorImager equipped with Molecular Dynamics Image software (Fuji).

Quantitative measurements of the IRE–IRP interaction by filter assay

Affinities of IRE–IRP interactions were measured for wild-type IRP-1 and different mutants by a filter assay. A constant amount of recombinant GST-tagged IRP-1 (50 or 100 ng) was incubated in microtiter wells for 10 min at 23°C with 10^4 c.p.m. [^{32}P]IRE (~15 pg) and increasing amounts of the same unlabeled IRE (500–6000 pg) in 100 µl of 10 mM HEPES pH 7.6, 3 mM $MgCl_2$, 40 mM KCl, 5% glycerol, 2% 2-mercaptoethanol. The mixture with IRE–IRP complexes was then filtered rapidly on a Minifold I dot-blot filtration apparatus (Schleicher & Schuell) across a nitrocellulose membrane, type BA79 (0.1 µm) (Schleicher & Schuell). Filters were washed twice with 50 mM NaCl, 10 mM Na phosphate pH 7.0 and dried. The retained radioactivity was quantified by autoradiography using a Compaq PhosphorImager (Molecular Dynamics). To diminish background, radiolabeled IRE was pre-filtered on a small Millipore 0.45 µm nitrocellulose filter, prior to the assay. For each labeled IRE batch, the protein-binding fraction was determined with an excess of wild-type IRP-1 (100, 500 or 1000 ng). Usually, at the two highest protein concentrations, a constant amount of 40–60% of the label was retained on the filter. For Scatchard plot analysis, this was considered as the total probe available. The background with [^{32}P]IRE alone, in the absence of IRP-1, was ~1% of the total radioactivity and subtracted from all measurements.

Aconitase assay

Aconitase activity was measured at 37°C by the disappearance of *cis*-aconitate at 240 nm (Drapier and Hibbs, 1986). The assay was performed with 10 µg freshly purified recombinant IRP-1 without thrombin cleavage in 50 mM Tris–HCl pH 7.2, 100 mM NaCl, 0.02% bovine serum albumin and an initial substrate concentration of 20–200 µM *cis*-aconitate (Sigma) in a 1 ml reaction volume.

Acknowledgements

We thank Tracey Rouault (NIH, Bethesda, MD) for making the human IRP-2 cDNA available and Manuel Peitsch (Glaxo, Geneva) for protein structure predictions**.** We are also grateful to Richard Iggo for carefully reading the manuscript. This project was supported by the Swiss National Science Foundation. P.K. was a recipient of fellowships from the European Community and the Roche Research Foundation.

References

Addess,K.J., Basilion,J.P., Klausner,R.D., Rouault,T.A. and Pardi,A. (1997) Structure and dynamics of the iron responsive element RNA: implications for binding of the RNA by iron regulatory binding proteins. *J. Mol. Biol.*, **274**, 72–83.

Basilion,J.P., Kennedy,M.C., Beinert,H., Massinople,C.M., Klausner, R.D. and Rouault,T.A. (1994a) Overexpression of iron-responsive element-binding protein and its analytical characterization as the RNA-binding form, devoid of an iron-sulfur cluster. *Arch. Biochem. Biophys.*, **311**, 517–522.

Basilion,J.P., Rouault,T.A., Massinople,C.M., Klausner,R.D. and Burgess,W.H. (1994b) The iron-responsive element-binding protein: localization of the RNA-binding site to the aconitase active-site cleft. *Proc. Natl Acad. Sci. USA*, **91**, 574–578.

Beinert,H., Kennedy,M.C. and Stout,C.D. (1996) Aconitase as iron-sulfur protein, enzyme and iron-regulatory protein. *Chem. Rev.*, **96**, 2335–2373.

Binder,R., Horowitz,J.A., Basilion,J.P., Koeller,D.M., Klausner,R.D. and Harford,J.B. (1994) Evidence that the pathway of transferrin receptor mRNA degradation involves an endonucleolytic cleavage within the 3′ UTR and does not involve poly(A) tail shortening. *EMBO J.*, **13**, 1969–1980.

Biou,V., Yaremchuk,A., Tukalo,M. and Cusack,S. (1994) The 2.9 Å crystal structure of *T. thermophilus* seryl-tRNA synthetase complexed with tRNASer. *Science*, **263**, 1404–1410.

Burd,C.G. and Dreyfuss,G. (1994) Conserved structures and diversity of functions of RNA-binding proteins. *Science*, **265**, 615–621.

Bycroft,M., Grünert,S., Murzin,A.G., Proctor,M. and St Johnston,D. (1995) NMR solution structure of a dsRNA binding domain from *Drosophila* staufen protein reveals homology to the N-terminal domain of ribosomal protein S5. *EMBO J.*, **14**, 3563–3571.

Casey,J.L., Hentze,M.W., Koeller,D.M., Caughman,S.W., Rouault,T.A., Klausner,R.D. and Harford,J.B. (1988) Iron-responsive elements: regulatory RNA sequences that control mRNA levels and translation. *Science*, **240**, 924–928.

Drapier,J.-C. and Hibbs,J.B.,Jr (1986) Murine cytotoxic activated macrophages inhibit aconitase in tumor cells. Inhibition involves the iron-sulfur prosthetic group and is reversible. *J. Clin. Invest*., **78**, 790–797.

Emery-Goodman,A., Hirling,H., Scarpellino,L., Henderson,B. and Kühn,L.C. (1993) Iron regulatory factor expressed from recombinant baculovirus: conversion between the RNA-binding apoprotein and Fe-S cluster containing aconitase. *Nucleic Acids Res.*, **21**, 1457–1461.

Frishman,D. and Hentze,M.W. (1996) Conservation of aconitase residues revealed by multiple sequence analysis. Implications for structure/function relationships. *Eur. J. Biochem*., **239**, 197–200.

Gdaniec,Z., Sierzputowska-Gracz,H. and Theil,E.C. (1998) Iron regulatory element and internal loop/bulge structure for ferritin mRNA studied by cobalt (III) hexammine binding, molecular modeling and NMR spectroscopy. *Biochemistry*, **37**, 1505–1512.

Gray,N.K., Quick,S., Goossen,B., Constable,A., Hirling,H., Kühn,L.C. and Hentze,M.W. (1993) Recombinant iron regulatory factor functions as an iron-responsive-element-binding protein, a translational repressor and an aconitase. A functional assay for translational repression and direct demonstration of the iron switch. *Eur. J. Biochem*., **218**, 657–667.

Guo,B., Yu,Y. and Leibold,E.A. (1994) Iron regulates cytoplasmic levels of a novel iron-responsive element-binding protein without aconitase activity. *J. Biol. Chem*., **269**, 24252–24260.

Guo,B., Brown,F.M., Phillips,J.D., Yu,Y. and Leibold,E.A. (1995) Characterization and expression of iron regulatory protein 2 (IRP2). Presence of multiple IRP2 transcripts regulated by intracellular iron levels. *J. Biol. Chem*., **270**, 16529–16535.

Haile,D.J., Rouault,T.A., Tang,C.K., Chin,J., Harford,J.B. and Klausner, R.D. (1992) Reciprocal control of RNA-binding and aconitase activity in the regulation of the iron-responsive element binding protein: role of the iron-sulfur cluster. *Proc. Natl Acad. Sci. USA*, **89**, 7536–7540.

Henderson,B.R., Seiser,C. and Kühn,L.C. (1993) Characterization of a second RNA-binding protein in rodents with specificity for iron-responsive elements. *J. Biol. Chem.*, **268**, 27327–27334.

Henderson,B.R., Menotti,E., Bonnard,C. and Kühn,L.C. (1994) Optimal sequence and structure of iron-responsive elements. Selection of RNA stem-loops with high affinity for iron regulatory factor. *J. Biol. Chem.*, **269**, 17481–17489.

Henderson,B.R., Menotti,E. and Kühn,L.C. (1996) Iron regulatory proteins 1 and 2 bind distinct sets of RNA target sequences. *J. Biol. Chem*., **271**, 4900–4908.

Hentze,M.W. and Kühn,L.C. (1996) Molecular control of vertebrate iron metabolism—mRNA-based regulatory circuits operated by iron, nitric oxide and oxidative stress. *Proc. Natl Acad. Sci. USA*, **93**, 8175–8182.

Hentze,M.W., Rouault,T.A., Harford,J.B. and Klausner,R.D. (1989) Oxidation-reduction and the molecular mechanism of a regulatory RNA–protein interaction. *Science*, **244**, 357–359.

Hirling,H., Emery-Goodman,A., Thompson,N., Neupert,B., Seiser,C. and Kühn,L.C. (1992) Expression of active iron regulatory factor from a full-length human cDNA by *in vitro* transcription/translation. *Nucleic Acids Res*., **20**, 33–39.

Hirling,H., Henderson,B.R. and Kühn,L.C. (1994) Mutational analysis of the [4Fe–4S]-cluster converting iron regulatory factor from its RNA-binding form to cytoplasmic aconitase. *EMBO J.*, **13**, 453–461.

Kenan,D.J., Query,C.C. and Keene,J.D. (1991) RNA recognition: towards identifying determinants of specificity. *Trends Biochem. Sci*., **16**, 214–220.

Kennedy,M.C., Mende-Mueller,L., Blondin,G.A. and Beinert,H. (1992) Purification and characterization of cytosolic aconitase from beef liver and its relationship to the iron-responsive element binding protein. *Proc. Natl Acad. Sci. USA*, **89**, 11730–11734.

Klausner,R.D., Rouault,T.A. and Harford,J.B. (1993) Regulating the fate of mRNA: The control of cellular iron metabolism. *Cell*, **72**, 19–28.

Koeller,D.M., Casey,J.L., Hentze,M.W., Gerhardt,E.M., Chan,L.-N., Klausner,R.D. and Harford,J.B. (1989) A cytosolic protein binds to structural elements within the iron regulatory region of the transferrin receptor mRNA. *Proc. Natl Acad. Sci. USA*, **86**, 3574–3578.

Kunkel,T.A., Roberts,J.D. and Zakour,R.A. (1987) Rapid and efficient site-specific mutagenesis without phenotypic selection. *Methods Enzymol*., **154**, 367–382.

Laing,L.G. and Hall,K.B. (1996) A model of the iron responsive element RNA hairpin loop structure determined from NMR and thermodynamic data. *Biochemistry*, **35**, 13586–13596.

Leibold,E.A. and Munro,H.N. (1988) Cytoplasmic protein binds *in vitro* to a highly conserved sequence in the 5′ untranslated region of ferritin heavy- and light-subunit mRNAs. *Proc. Natl Acad. Sci. USA*, **85**, 2171–2175.

Müllner,E.W. and Kühn,L.C. (1988) A stem-loop in the 3′ untranslated region mediates iron-dependent regulation of transferrin receptor mRNA stability in the cytoplasm. *Cell*, **53**, 815–825.

Müllner,E.W., Neupert,B. and Kühn,L.C. (1989) A specific mRNA-binding factor regulates the iron-dependent stability of cytoplasmic transferrin receptor mRNA. *Cell*, **58**, 373–382.

Musco,G., Stier,G., Joseph,C., Castiglione Morelli,M.A., Nilges,M., Gibson,T.J. and Pastore,A. (1996) Three-dimensional structure and stability of the KH domain: molecular insights into the fragile X syndrome. *Cell*, **85**, 237–245.

Nagai,K. (1996) RNA–protein complexes. *Curr. Opin. Struct. Biol*., **6**, 53–61.

Neupert,B., Menotti,E. and Kühn,L.C. (1995) A novel method to identify nucleic acid binding sites in proteins by scanning mutagenesis—application to iron regulatory protein. *Nucleic Acids Res*., **23**, 2579–2583.

Oubridge,C., Ito,N., Evans,P.R., Teo,C.H. and Nagai,K. (1994) Crystal structure at 1.92 Å resolution of the RNA-binding domain of the U1A spliceosomal protein complexed with an RNA hairpin. *Nature*, **372**, 432–438.

Patino,M.M. and Walden,W.E. (1992) Cloning of a functional cDNA for the rabbit ferritin mRNA repressor protein. Demonstration of a tissue-specific pattern of expression. *J. Biol. Chem*., **267**, 19011–19016.

Peyret,P., Perez,P. and Alric,M. (1995) Structure, genomic organization and expression of the *Arabidopsis thaliana* aconitase gene: plant aconitase shows significant homology with mammalian iron-responsive element-binding protein. *J. Biol. Chem*., **270**, 8131–8137.

Philpott,C.C., Rouault,T.A. and Klausner,R.D. (1991) Sequence and expression of the murine iron-responsive element binding protein. *Nucleic Acids Res*., **19**, 6333.

Philpott,C.C., Haile,D., Rouault,T.A. and Klausner,R.D. (1993) Modification of a free Fe-S cluster cysteine residue in the active iron-responsive element-binding protein prevents RNA binding. *J. Biol. Chem*., **268**, 17655–17658.

Philpott,C.C., Klausner,R.D. and Rouault,T.A. (1994) The bifunctional iron-responsive element binding protein/cytosolic aconitase: the role of active-site residues in ligand binding and regulation. *Proc. Natl Acad. Sci. USA*, **91**, 7321–7325.

Prodromou,C., Artymiuk,P.J. and Guest,J.R. (1992) The aconitase of *Escherichia coli*. Nucleotide sequence of the aconitase gene and amino acid sequence similarity with mitochondrial aconitases, the iron-responsive-element-binding protein and isopropylmalate isomerases. *Eur. J. Biochem*., **204**, 599–609.

Robbins,A.H. and Stout,C.D. (1989) The structure of aconitase. *Proteins*, **5**, 289–312.

Rothenberger,S., Müllner,E.W. and Kühn,L.C. (1990) The mRNA-binding protein which controls ferritin and transferrin receptor expression is conserved during evolution. *Nucleic Acids Res*., **18**, 1175–1179.

Rouault,T.A., Tang,C.K., Kaptain,S., Burgess,W.H., Haile,D.J., Samaniego,F., McBride,O.W., Harford,J.B. and Klausner,R.D. (1990) Cloning of the cDNA encoding an RNA regulatory protein: the human iron-responsive element-binding protein. *Proc. Natl Acad. Sci. USA*, **87**, 7958–7962.

Rouault,T.A., Stout,C.D., Kaptain,S., Harford,J.B. and Klausner,R.D. (1991) Structural relationship between an iron-regulated RNA-binding protein (IRE-BP) and aconitase: functional implications. *Cell*, **64**, 881–883.

Rouault,T.A. *et al.* (1992) An iron-sulfur cluster plays a novel regulatory role in the iron-responsive element binding protein. *BioMetals*, **5**, 131–140.

Samaniego,F., Chin,J., Iwai,K., Rouault,T.A. and Klausner,R.D. (1994) Molecular characterization of a second iron-responsive element binding protein, iron regulatory protein 2: structure, function and post-translational regulations. *J. Biol. Chem.*, **269**, 30904–30910.

Sanger,F., Nicklen,S. and Coulson,A.R. (1977) DNA sequencing with chain-terminating inhibitors. *Proc. Natl Acad. Sci. USA*, **74**, 5463–5467.

Schalinske,K.L., Anderson,S.A., Tuazon,P.T., Chen,O.S., Kennedy,M.C. and Eisenstein,R.S. (1997) The iron-sulfur cluster of iron regulatory protein 1 modulates the accessibility of RNA binding and phosphorylation sites. *Biochemistry*, **36**, 3950–3958.

Schlegl,J., Gegout,V., Schlager,B., Hentze,M.W., Westhof,E., Ehresmann,C., Ehresmann,B. and Romby,P. (1997) Probing the structure of the regulatory region of human transferrin receptor messenger RNA and its interaction with iron regulatory protein-1. *RNA*, **3**, 1159–1172.

Siomi,H., Choi,M., Siomi,M.C., Nussbaum,R.L. and Dreyfuss,G. (1994) Essential role for KH domains in RNA binding: impaired RNA binding by a mutation in the KH domain of FMR1 that causes fragile X syndrome. *Cell*, **77**, 33–39.

Smith,D.B. and Johnson,K.S. (1988) Single-step purification of polypeptides expressed in *Escherichia coli* as fusions with glutathione *S*-transferase. *Gene*, **67**, 31–40.

Uhlenbeck,O.C., Pardi,A. and Feigon,J. (1997) RNA structure comes of age. *Cell*, **90**, 833–840.

Valegard,K., Murray,J.B., Stockley,P.G., Stonehouse,N.J. and Liljas,L. (1994) Crystal structure of an RNA bacteriophage coat protein–operator complex. *Nature*, **371**, 623–626.

Yu,Y., Radisky,E. and Leibold,E.A. (1992) The iron-responsive element binding protein. Purification, cloning and regulation in rat liver. *J. Biol. Chem*., **267**, 19005–19010.

Zheng,L., Andrews,P.C., Hermodson,M.A., Dixon,J.E. and Zalkin,H. (1990) Cloning and structural characterization of porcine heart aconitase. *J. Biol. Chem*., **265**, 2814–2821.

Received August 13, 1998; revised September 14, 1999; accepted September 15, 1999